Radar-based assessment of hail frequency in Europe

Elody Fluck[1,*], Michael Kunz[1,2], Peter Geissbuehler[3], and Stefan P. Ritz[3]

[1]Institute of Meteorology and Climate Research (IMK), Karlsruhe Institute of Technology (KIT), Karlsruhe, Germany
[2]Center for Disaster Management and Risk Reduction Technology (CEDIM), Karlsruhe, Germany
[3]RenaissanceRe Europe AG, Zurich, Switzerland
[*]now at: Department of Earth and Planetary Sciences, Weizmann Institute of Science, Rehovot, Israel

Correspondence: Elody Fluck (elody.fluck@weizmann.ac.il)

Abstract.

In this study we present a unique 10-year climatology of severe convective storm tracks for a larger European area covering Germany, France, Belgium, and Luxembourg. For the period 2005-2014, a high-resolution hail potential composite of 1×1 km^2 is produced from two-dimensional reflectivity radar data and lightning data. Individual hailstorm tracks as well as their physical

5 properties, such as radar reflectivity along the tracks were reconstructed for the entire time period using the Convective Cell Tracking Algorithm (CCTA2D).

A sea-to-continent gradient in the number of hail days is present over the whole domain. In addition, the highest number of severe storms is found on the leeward side of low mountain ranges such as near the Massif Central in France and the Swabian Jura in southwest Germany. A latitude shift in the hail peak month is observed between the northern part of Germany where hail

10 occurs most frequently in August, and southern France where the maximum of hail occurs two months earlier. The spatially most extended footprints with high reflectivity values occurred on 9 June 2014 and on 28 July 2013 with lengths reaching several hundreds of kilometers. Both events implied hailstones measuring up to 10 cm which caused damage in excess of 2 Billions Euros.

1   Introduction

15 Severe convective storms (SCS) and related hail constitute a major atmospheric hazard. These events have the potential to cause substantial damage to property such as buildings or automobiles in various parts of Europe, including southern France, Germany, Austria, and Switzerland (for example: Dessens, 1986; Puskeiler et al., 2016; Nisi et al., 2016). Prominent examples are the two hailstorms related to the low-pressure system Andreas that occurred on 27/28 July 2013 over central and southern Germany with total economic losses estimated to approximately EUR 3.6 billion (SwissRe, 2014,Kunz et al., 2018). A major

20 obstacle when investigating hail events and their climatology, respectively, is the lack of accurate and comprehensive observations. This is due to the local-scale nature of SCS and the even smaller hailstreaks with a small spatial extent (Changnon, 1977). There are only a few regional-scale ground detection networks using hailpads for recording hail fall in operation, such as in southwestern and central France (Dessens, 1986, Vinet, 2001) or parts of Spain (Fraile et al., 1992). The major part of

Europe, however, remains uncovered by a hail network leading to a gap in direct hail observations. Therefore, little is known
25   about the local-scale hail probability and related hail risk across Europe.

Numerous authors used hail signals derived from conventional weather radars for the identification and analysis of hail
because of their high temporal and spatial resolutions. For example, Nisi et al. (2016) and Nisi et al. (2018) established a
hail climatology for Switzerland from 2002 to 2014 based on both Probability of Hail (POH) and Maximum Expected Severe
Hail Size (MESHS) estimated from volumetric (3D) radar data.Puskeiler et al. (2016) used 3D radar reflectivity together with
30   modelled melting layer, lightning data and the cell-tracking algorithm TRACE3D (Handwerker, 2002) to reconstruct hailstreaks
and, from that, to estimate the hail frequency across Germany between 2004 and 2014. Combining 3D radar reflectivity and
insurance loss data for buildings, Kunz and Puskeiler (2010) found the highest hail frequency in Southwest Germany to be
located downstream of the Black Forest mountains. This hot spot was also confirmed by Kunz and Kugel (2015) using five
different hail criterions based on 2D and 3D radar reflectivities and different heights (melting layer, echotop). Lukach et al.
35   (2017) computed a hail frequency map for Belgium from 2003 to 2012 using 3D radar data. Despite the use of improved radar-
based techniques, most of the studies cited above were restricted to smaller regions or a single country. While some authors
have estimated hail frequency from other methods such as Overshooting Top (OT) detections in satellite imagery (Punge et al.,
2014), model data (Mohr et al., 2015b, a; Rädler et al., 2018) or a combination thereof (Punge et al., 2017), these methods
are not as straight forward as those based on radar reflectivity. Numerical models, such as weather forecast or regional climate
40   models (RCM), on the other hand, are not able to reliably reproduce convective storms and associated phenomena such as hail
due to a high degree of uncertainty in the initial conditions, a lack of knowledge in cloud microphysics, and the high computer
costs when running a two- or three-moments microphysics scheme.

The objective of our study is to analyze the spatiotemporal variability of hail signals over a 10-year period (2005 to 2014)
covering the four European countries of France, Germany, Belgium and Luxembourg. Hail signals were estimated from 2D
45   radar reflectivity available for each country, which permitted a homogeneous hail analysis. The results help to identify regions
frequently affected by hail and allows us to relate hail frequency to topographic features such as terrain height or the proximity
to the Sea. A thorough study of hail events may give further insights into the mechanisms driving the onset of deep moist
convection. Improved understanding of these mechanisms and processes is crucial to improve the nowcasting and forecasting
skill of hail storms. Finally, as hail constitutes a considerable risk for the insurance industry, improved knowledge about hail
50   frequency, intensity, and hailstorm characteristics will help to better understand the related risks.

The paper is structured as follows: Section 2 gives an overview of the remote-sensing datasets used for this study. Section 3,
describes the combination of radar data with lightning data and the application of the tracking algorithm. The remote-sensing
output is then used to generate European composites at 5-minute time steps. Section 4 assesses the hail variability between
2005 to 2014 in relation to the distance to the sea and the presence of orography near hailstorms. Concluding remarks follow
55   in Section 5.

2 Datasets

2.1 Remote-sensing data

In this study, 2D radar reflectivity data for the summer half-years (April to September) from 2005 to 2014 for Germany, France, Belgium, and Luxembourg are considered (Figure 1). The radar products investigated are composites of the Maximum Constant Altitude Plan Position Indicator (MaxCAPPI), where the composite is a merger of the data from all local radar stations in a single image at time steps of five minutes. 2D radar data are used here because of the large domain and their long-term availability.

2.1.1 French radar data

The French radar network operated by Météo-France included 29 radar stations in 2015 with 19 C-band radars, five S-band radars (both with a radius of up to 120 km), as well as five X-band radars with an average coverage radius of 50 km (Figure 2). As the X-band radar data were only recently implemented into the French national composite (Yu et al., 2018), only S- and C-band radars were considered in this study. The radar coverage provided by the two stations of Avesnois (located in North France) and Réhicourt-la-petite in the Lorraine region (Figure 1) cover a large part of Eastern France, and permit to integrate Luxembourg completely, as well as a significant part of Belgium into the French national composite. The French national mosaic represents instantaneous reflectivity with a resolution of 1×1 km^2 every 5 minutes, which leads to a composite size of 1536×1536 grid points for each image (Tabary, 2007).

Radar data quality has been checked several times for the French radar network, like Gourley et al. (2006), who proceeded to a quality check of C-band radars. Furthermore, a radar correction algorithm including beam-blocking correction and ground-clutter identification was applied on the French reflectivity mosaic (Tabary, 2007). Reflectivity values were coded in a table and stored for the period from 1999 to 2014 in GeoTIFF format, i.e., georeferenced TIFF images. The resolution is 2×2 km^2 from 1999 until mid-June 2009, and a finer resolution of 1×1 km^2 is available from the end of July 2009 to 2014. For data homogenization, each of the 2×2 km^2 composite was interpolated linearly from 1999 to July 2009 to the finer grid of 1×1 km^2.

2.1.2 German radar data

The German radar composites for the period 2005 to 2014 is provided by the German Weather Service (DWD), which operated a network of 17 C-band radar systems in 2016. As the horizontal range detection for each radar station is 180 km and a maximum distance of 200 km separates the radar stations, the extensive overlap of the detection areas permits almost a complete coverage of the German territory. Only some peripheral regions of Germany remain as a gap in the composite, for example, in the far north near the Danish border or in southeastern Bavaria (Figure 2). In the complex terrain of southern Germany, weather radars are preferably located on hills and mountain to minimize the shading effects induced by orography. The spatiotemporal resolution of the composite is the same as of the French national composite, namely 1×1 km^2 and 5-minute. Moreover, the same period (2005 to 2014) was chosen as for the French mosaic allowing for merging and comparison of both datasets. The

encryption of each scan of the DWD network entails raw terrain-following near ground reflectivity (CAPPI) values (so-called RX product) in so-called RVP6 units. The conversion from RVP6 to dBZ is performed as follows:

$$X \text{ dBZ} = (\frac{RVP6}{2} - 32.5) \text{ dBZ} \tag{1}$$

90   The accuracy of the RVP-6 units is 0.5 dBZ in a range from 0 to 255. This corresponds to a reflectivity from -32.5 to 95 dBZ. The advantages of this data is certainly the high temporal and spatial resolution, which enables proper identification of SCS, as well as the low increments. The German radar composite includes an equidistant field size of $900 \times 900 \text{ km}^2$ covering the whole of Germany. The coordinate system of the national composite consists of a polar stereographic projection, so that each grid box in the projection is equidistant at 1.0 km.

2.1.3   Uniform Pan-European Grid

The radar reflectivity data or the climatology of radar-derived hail signals, respectively, were projected on the same uniform European grid (not shown) with a resolution identical to that of the national radar network ($1 \times 1 \text{ km}^2$). The grid uses the standard coordinate system and the standard spheroidal reference surface defined by the World Geodetic System elaborated in 1984 (WGS84). In the center at about 47°N and 6°E, the meridional grid spacing is equal to the zonal direction to minimize 100   the grid distortion.

2.1.4   Lightning data

To remove still present artificial clutter, we filtered the radar data with lightning data. Here we used cloud-to-ground (CG) light-ning (strokes) from the ground-based low-frequency lightning detection system BLIDS (BLitz InformationsDienst Siemens), which is part of the EUCLID (EUropean Cooperation for LIghtning Detection) network. The detection efficiency of the system 105   is 96% for strokes with a peak current of at least 2 kA (Schulz et al., 2016). Since the operational system and the algorithm implemented until 2015 had a significantly lower detection efficiency of intra-cloud and cloud-to-cloud lightning according to Pohjola and Mäkelä (2013), these types were not considered.

3   Methods

3.1   Data processing

110 Concerning the homogenization of the French and German national composites, several corrections had already been performed by both meteorological services. Radar reflectivity data still contains noise and systematic errors that have to be eliminated us-ing various approaches. Errors mostly concern individual grid points with significant high reflectivity (e.g., more than 70 dBZ) compared to the surroundings. To avoid this problem, only reflectivity in the range of 35 to 70 dBZ was considered in the analyses. A verification and correction filter was applied for values larger than 45 dBZ: when an individual grid point had a

significantly higher value (difference greater than 5 dBZ) compared to all its surroundings within a range of 2 km, its value $Z(x,y)$ was set to the mean value of the surrounding grid points (Puskeiler et al., 2016).

$$Z(x,y) = \frac{1}{8}\left(\sum_{i=-1}^{1}\sum_{j=-1}^{1} Z(x+i, y+j) - Z(x,y)\right) \tag{2}$$

This filter was applied to all consecutive radar scans. When a high reflectivity value only occurred during a single time step and not before or afterward, it was considered an artifact and removed. Reflectivity values near neighboring countries were evaluated and calibrate with radar stations close to the border.

3.2 Lightning filter

Despite the radar tracking routine (see next paragraph) has included a clutter filter, several erroneous signals are still present in the radar data. Such high reflectivity echoes can, for example, appear when the radar beam hits lightning during a storm (Ligda, 1956; Caylor and Chandrasekar, 1996). The ionized lightning combined with high temperatures lead to a specific reflection of the transmitted radar beam to the antenna. Since hail occurs only in connection with thunderstorms (Baughman and Fuquay, 1970; Changnon, 1999; Wapler, 2017), presumably lightning can also be detected near a hail signal, i.e. large reflectivities. Thus, the plausibility of the radar products can be checked and corrected using lightning data. If high reflectivity during a day occurs without lightning, the values at the affected grid points are set to zero. A maximum distance of 10 km was chosen between a lightning discharge location and the grid points with high reflectivity. Distances of 5, 15, and 20 km were also tested; a distance of 5 km led to the disruption of several hail trajectories due to gaps in reflectivity values; the other two thresholds affected the results only marginally.

3.3 The convective cell tracking algorithm CCTA2D

The object-based Convective Cell Tracking Algorithm (CCTA2D) permits the reconstruction of trajectories of individual convective cells using 2D radar data. The algorithm is based on TRACE3D (Handwerker, 2002), originally developed and optimized for 3D radar reflectivity from a single radar in spherical coordinates. The original version of TRACE3D was further extended to radar reflectivity data in Cartesian coordinates such as those provided by the DWD radar network (Puskeiler et al., 2016). In addition, a second version was developed using 2D radar products by considering a unique elevation level at the surface and by enlarging the domain to all of Germany. Finally, CCTA2D was further extended and adapted in this study to the mosaic including France, Belgium, and Luxembourg (Fluck, 2018).

The first step of the CCTA2D processing is to identify convective cells with reflectivity values of at least 55 dBZ, denoted to as reflectivity core (RC), and to distinguish individual cells using different sub-thresholds. The 55 dBZ threshold is referred to as the criterion according to Mason (1971) successfully used in several studies (Hohl, 2001; Hohl et al., 2002; Kunz and Kugel, 2015, e.g.,). Schuster et al. (2005), for example, found the 55 BZ to be a good indicator for damaging hail on the ground in Eastern Australia. Puskeiler et al. (2016) estimated a slightly higher threshold of 56 dBZ best separating between days with and without damage to buildings. Categorical verification using insurance loss data over a 7-years period in southwest Germany

for this threshold yields a Heidke Skill Score HSS of 0.6, a quite high value confirming the detection skill (it should be noted that this value increases to HSS = 0.71 when using an adjusted version of the Waldvogel et al. (1979) criterion requiring 3D radar data).

150   The second step CCTA2D is the temporal and spatial tracking of all detected convective cells. The algorithm assigns the RC of the former radar composite to the recent composite according to the estimated progagation velocity and position of the RC. Prerequisite of the tracking is that similarities between different RCs, for example, in intensity and size, from one time step to the next, must exist within a certain search radius for accurate RC assignment and tracking. The search radius is given by the estimated distance of an initial RC displaced during a time step of 5 min multiplied by a velocity factor of 0.6.

    Special attention is given to cell splitting and merging. To detect a splitting, the initial RC is first spatially displaced to the

155   position of the following RC (e.g., the successor), and their respective areas are compared. If the area of the successor differs significantly from the initial RC, it is assigned a potential splitting. In the case of merging, the opposite calculation from cell splitting is performed. Initial and successor areas are then compared, and the successor is placed at the weighted center of all initial detected cores. Merging occurs when the successor area is larger than the initial RC. To avoid reflectivity core crossings or overlapping, each RC is enumerated and recorded separately.

160   After the reconstruction of entire tracks, the composite of maximum reflectivity on a given day does not provide a smooth result, but a rather scattered product. This effect is most pronounced when the cells propagate further than their horizontal extent during a measuring interval. The faster the storms, the more scattered is the maximum reflectivity projected on a 2D plane. This can result in substantially reduced reflectivity values between two scans, even though a high-intensity storm crossed the area. To account for this effect, an advection correction was performed following Puskeiler et al. (2016). A translation of

165   the reflectivity cores is computed from one time step to the next considering the horizontal wind field estimated by CCTA2D along a track. Horizontal wind components, as well as the track direction of a thunderstorm, are computed and projected on the German and French grid. Each point along a track includes a velocity shift-vector in north-to-south (dv) and west-to-east (du) directions.

    Tests with long-living SCS tracks were compared with hail reports archived by the European Severe Weather Database

170   (ESWD) operated by the European Severe Storms Laboratory (Dotzek et al., 2009) along the reconstructed storm trajectories to assess the reliability of CCTA2D (not shown). In most cases, the ESWD reports were located close to the center of SCS tracks.

4 Results

4.1 Spatial distribution of hail

175 Figure 3 presents the hail probability map for the radar domain in terms of the number of hail days during the period 2005 to 2014 with a resolution of 1×1 km^2 based on 2D radar reflectivity. A day with hail is considered when the threshold of 55 dBZ is exceeded in the daily maximum reflectivity composite after (i) data correction, (ii) filtering with lightning data, and (iii) tracking with the object oriented algorithm CCTA2D as described in the previous section. If the lower threshold of 55 dBZ on

a specific day is reached at a single grid point, the hail field is set to 1, otherwise it is counted as zero. The sum over the entire
180 period of 10 years × 183 days (summer half-year) yields the radar-based climatology. Note that this climatology represents the
spatial distribution of convective cells with high reflectivity, but not directly of hail. The term hail days used in the following
refers to the exceedance of reflectivity, but not to confirmed hail observations.

As can be seen in Figure 3, the spatial variability of hail days is very large, but some patterns with distinct minima or maxima
can be identified. The area with the highest number of hail days is situated in central France on the northern flank of the Massif
185 Central (Figure 4) accumulating up to 46 hail days during the 10-year investigation period. Hailstorms in Western Europe are
associated mostly with southwesterly winds, but local-scale, thermally or dynamically-driven wind circulations from different
directions can interact with the dominant southwestern flow (Merino et al., 2013). Important is the geographical location of
the Massif Central and its shape (in the continent, perpendicular to the dominant flow). It is the first natural barrier from the
Mediterranean, and air flow advected from there can transport warm and moist air along the Rhone Valley, by channeling
190 and accelerating along valleys situated southeast of the Massif Central. These valleys are oriented on a northwest-to-southeast
axis and permit the Mediterranean flow to circulate along the entire valley (Bastin et al., 2005). The Massif Central can also
be affected by a cold low-level wind (mistral) coming from northwest to southern directions and transporting dry and cold
continental air over the Limagne Plain, thus leading to blocking at the windward side of the foothills of the Livradois and
Aubrac mountains, where hailstorms frequently occur.

195 A close-up investigation of the hail hot spots shows that the maximum of 46 hail days occurs on the southwestern flank of
the Livradois (Figure 4) situated between the Aubrac and the Forez mountains and extending over a few kilometers from the
northwest to the southeast. The location of the latter maximum shows an interaction between several factors that result in the
triggering of hailstorms in that specific region. Most of the valleys located southwest of the Massif Central are oriented from
southwest to northeast, thereby permitting a continuous transport of moist air from the Atlantic Ocean. The V-shaped valleys
200 lead to enhanced upward motions and favor terrain-forced convection. The strength of the updrafts depends on the diurnal
thermal circulation (and, of course, the terrain's slope). During the afternoon, the flow may go along the Aubrac Mountains
and along the slopes of the volcanoes (Chaîne des Puys) located on the western flanks of the mountain range. The air that is
forced to flow over the higher mountains may generate generates gravity waves on the leeward side of the mountain (Chappell,
1986), an area of lower pressure, enhanced turbulence, and periodic vertical displacement of fluid parcels. The combination
205 of increased vertical wind shear due to flow deviations at obstacles, and low-level flow convergence, and increased moisture
at lower levels may lead to favorable conditions for the triggering of convection downstream of the mountains (Kunz and
Puskeiler, 2010).

The northeastern part of France, including the regions of Burgundy, Champagne-Ardenne, Lorraine and France-Comté
(Figure 1), are affected with a maximum of 31 hail days in the central part of Burgundy, and more precisely on the eastern side
210 of mountains ranging from approximately 300 to 900 m (named Morvan range). In Champagne-Ardenne, the region flanking
Burgundy on its northeast boarder, the number of hail days reach up to 29 days over the mainly rolling terrain. In Lorraine,
where the terrain is almost flat and the climate is more continentally characterized, on average 27 hail days were counted in its
central part. A local and weaker maximum of 24 hail days can be recognized at the southeast edge of Lorraine on the windward

side of the Vosges mountains, representing an area with complex terrain with mountains of up to 1.424 m agl (Grand Ballon).
The height of these secondary mountain ranges is slightly higher in the southern part of Lorraine compared to the north. The
north-to-south orientation of the Vosges in addition to the higher elevation represent a natural obstacle opposed to the main
southwesterly flow, and may help convective clouds to develop in southwestern Alsace.

Another hail hotspot in the northeast part of France is found along the northern ridge of the Jura Mountains in east of France-
Comté with 25 hail days. The western part of the region is mainly flat and includes the Doubs Valley. The Jura mountains
represent a natural obstacle which may trigger thunderstorms and hailstorms by orographical lifting.

The Rhone-Alpes is a region likewise frequently affected by hail. This region contains the large Rhone valley and is bordered
by the Massif Central in the west and by the Alps to the east. The southwestern part as well as the southeastern edge of the
region show a local hail maximum with up to 31 hail days. The existence of these two hot spots can be explained by their
proximity to the Mediterranean as during southerly flows, warm and moist air is advected preferably through the Rhone valley.
The warm and moist air can then be lifted, for example, near a front system crossing the country from northwest to southeast,
leading to forced convection.

Southwestern France, including both the Aquitaine and Midi-Pyrenees regions, is also frequently affected by hail with up to
26 hail days in the southwest range of the Massif Central. Aquitaine and Midi-Pyrenees regions are the two regions well known
in the literature for their high hail probability (Vinet, 2001; Punge et al., 2014). Hermida et al. (2015) recently used data from
the ANELFA (Association Nationale d'Etude et de Lutte contre les Fléaux Atmosphériques) hailpad network and found that
the Gers Department, located on the west side of the Midi-Pyrenees region, is the area most affected by hail in southwestern
France.

The western and northern sides of the Pyrenees are also frequently affected by hail with up to 25 hail days. Although the
leeward side of the mountain range shows an increased hail frequency, the hail potential in the central parts is very low with
around 2 hail days close to the summits of the Pyrenean mountain range. According to Berthet et al. (2011), hail in that region
frequently occurs when a low-pressure system is located over the western part of Spain leading to southwesterly flow over
France associated with the advection of warm and moist air over the Pyrenean mountain range. The central part of the Pyrenees
possesses a high number of north-to-south valleys (orthogonal to the mean wind) that may affect local wind regimes, which in
turn are strengthened in sharp valleys and permit substantial orographic lifting.

The main hail hotspot in Germany is located in the southwest part of the country in the federal State of Baden-Württemberg,
specifically over the Swabian Jura, south of the city of Stuttgart, with a maximum of 31 hail days. This hotspot has already
been identified in previous studies of Puskeiler (2013) and Junghänel et al. (2016). During days with damaging hail, Kunz
and Puskeiler (2010) found a Froude number below 1 in this region, indicating a flow-around regime at low levels of the
Southern Black Forest rather than over it, causing a zone of horizontal flow convergence downstream. This convergence zone
coincides with the area of the highest number of hail days (Kunz and Puskeiler, 2010; Koebele, 2014). Moreover, Kunz and
Puskeiler (2010) hypothesized that the southwesterly flow meets the Swabian Jura at a very sharp angle, which reduces the
Froude number considerably and forces the wind to flow parallel to the mountain chain. This flow modification is assumed to
be responsible for the flow convergence at low levels as observed, for example, by Koebele (2014).

Weaker maxima in hail frequency with a mean of 11 hail days are found north of the Alps in the State of Bavaria. The

250   north-to-south, pre-Alpine-orientated valleys in this region may lead to flow deviations and low level convergence, similarly to the Swabian Jura area. However, also Alpine pumping, a secondary mountain-plain circulation (Weissmann et al., 2005) leading to flow towards the Alps and creating convergence zones, may play a decisive role for this distribution (Nisi et al., 2018).

In the northeast of Germany, a local maximum of up to 32 hail days is positioned over the Saxon Ore Mountains south of

255   the city of Dresden. Note, however, that this maximum is mainly caused by a high number of SCS in the year of 2007 (Piper, 2017), which was characterized by frequent upper air troughs over Western Europe and ridges over Central Europe, leading to high-pressure gradients on the eastern part of Germany and a southeast-to-northeast flow regime from the Czech Republic (note that the almost same situation occurred in 2019). The northwestern part of Germany, including the States of Hesse and Rhineland-Palatinate, and the southern part of North Rhine-Westphalia are regions affected by approximately 14 days with

260   hail. The location of the hail patterns is partly caused by the local orography. The pronounced maximum in North Hesse lies directly to the east and thus partly at the leeward side of the Westerwald, which is characterized by rolling terrain.

In contrast to the various hail hot spots located exclusively in the continental domain and preferably along the mountain's foothills, most of the minima are found along the coastlines where hail is also a year-round phenomenon (Dessens, 1986). Hail is rare along the Atlantic as well as Mediterranean coasts, where the latter counts up to 2 hail days in its southern region. The

265   large heat capacity of the water reduce the diurnal cycle of temperature leading to a decrease in the lapse rate magnitude. As a result, the sea contributes to the inhibition of SCS development, even if the increased moisture content of the atmosphere near the coasts provides a source of energy for the storms (Piper and Kunz, 2017).

4.2   Annual variability

The annual frequency of thunderstorms or hailstorms, respectively, show a very large annual and multi-annual variability

270   (e.g., Puskeiler et al., 2016; Nisi et al., 2018). As shown by Piper et al. (2019), this variability is partly related to large-scale mechanisms such as the presence of specific Northern Hemisphere Teleconnection patterns representing the low-frequency mode of the climate system (e.g., North Atlantic Oscillation NAO or East Atlantic pattern) or by variations in the sea surface temperature (SST). Having reconstructed a very large event set of SCS/hailstorms, we are also interested how the frequency of these events vary across the whole domain and regionally.

275   Annual mean frequency anomalies were computed by averaging all hail days over the entire investigation area for each year between 2005 and 2014 (Figure 5) and subtracting the mean number of hail days of the entire period. Positive or negative values represent higher or lower numbers, respectively, of hail days compared to the 10-year average. As shown in Figure 5 the annual variability is very high and without any trend.

The absolute maximum of hail days is reached in 2006 (+1.27 hail days compared to the average of 2.32). During that year,

280   large parts of Europe, including Germany, Belgium, Luxembourg, and northwest France, experienced higher temperatures, especially during the end of June and July, when two heat waves occurred (Fouillet et al., 2008). As a result, Mediterranean SST showed a positive anomaly, leading to intense evaporation rates, and, consequently, to an increase in the amount of water

vapor in the atmosphere. In addition, large-scale lifting (e.g., related to differential vorticity advection) could have led to an increase in convective available potential energy (CAPE) and a low convective inhibition (CIN). The combination of high

285 moisture in the boundary layer, low CIN, high CAPE and lifting mechanisms may give rise to a substantial increase in SCS. The spatial distribution of hail days in 2006 (Figure 6) strongly resemble the climatology, with several maxima near hilly terrains and minima near coastlines. Some hot spots can also be highlighted over the northwest part of France and in Southwestern Germany.

The year with the second highest number of hail days is 2012. The positive anomaly of hail days (+1.17) was mainly related
290 to an intense thunderstorm activity especially over Southwestern Germany and France during the end of June and in July (DeutscheRück, 2013).

By contrast, the year of 2010 shows the lowest number in hail days (anomaly -1.25). Even though 2010 was very warm worldwide (NOAA, 2011), summer temperature in parts of Europe including Germany were below average. Furthermore several persistent large-scale ridges may have suppressed the formation of hailstorms (DeutscheRück, 2013). No clear spatial
295 pattern can be found during 2010; only a few hailstorms occurred in Central France that year. There was almost no hail from an axis Northwest France to North Germany. The regions where hail was less present compared to the mean, are located over the entirety of Belgium, Luxembourg, and the northwest of France, especially Normandy and Brittany, which were not affected by hail, and along the coastlines.

Also the year of 2013 shows a negative anomaly, which is somewhat surprising because it is also the year with the largest
300 damage caused by hailstorms in Germany. For example, clusters of SCS that formed in relation to the low pressure Andreas caused an economic loss of EUR 3.6 billion (Kunz et al., 2018). June 2013 was colder than average in West Europe (NOAA, 2014) and a severe flood affected Germany rather. In addition, the thunderstorm activity of 2013 was lower than the mean (Piper, 2017). Negative anomalies in hail frequency are also seen in the years of 2014 (-1.03) and 2005, where the latter remains unclear since some radar data were missed in Germany for April.

305 ## 4.3 Seasonal and diurnal cycles of SCS

The large spatiotemporal variability of hail discussed in the previous sections leads us to investigate the seasonal and diurnal cycle of SCSs at a regional scale. To better understand the characteristics of the events and the mechanisms that favor the development of hailstorms, the total area under investigation was divided into 13 subdomains of approximately similar size (around 75,000 km^2) framed in Figure 3. We selected five subdomains for further discussion: 3=NBEL (North of Belgium),
310 7=IDF (Ile-de-France), 9=BAVAR (Bavaria), 11=MCEN (Massif Central) and 12=MAQUI (Midi-Pyrenees and Aquitaine) representing different terrain and climatological characteristics. The coastal subdomains NBEL, IDF and MAQUI have a climate influenced mainly by maritime air masses. Subdomains NBEL and IDF are flatlands, while subdomain MAQUI contain the Pyrenean large mountains. Subdomains BAVAR and MCEN have a climate somewhat characterized more to be continentally, but differ in the characteristics of their orography: Hilly terrains characterize subdomain BAVAR, whereas subdomain MCEN
315 includes several mountains of the Massif Central.

To quantify the number of hail days for each of the subdomains, the number of hail days of all grid points was accumulated 7. Despite the large variability inherent in these graphs, some similarities can be recognized. All time series of the different subdomains feature a clear annual cycle with a minimum of hail days in spring and autumn and a maximum during the summer. This characteristic cycle of hail days with a strong increase in the frequency during April/May and a significant decrease around

320 September, and with a maximum during the summer was found by several other authors such as Dessens (1986) and Vinet (2002) for France, Belgium and Luxembourg, by Gudd (2003), Deepen (2006), Mohr and Kunz (2013) and Puskeiler et al. (2016) for Germany, and by Nisi et al. (2014) and Nisi et al. (2018) for Switzerland and northern Italy.

Mountainous subdomain MCEN shows the largest number of hail days and has the most pronounced annual cycle. Until the end of April, the number of hail days does not exceed 200 in this subdomain. During May and beginning of June, the

325 number increases substantially from 281 for the 10-day average centered around 10 May up to 453 days on 9 June. The more pronounced diurnal temperature cycle for continental regions, associated with a higher lapse rate in combination with orographic lifting may explain this increase (Berthet et al., 2011). The overall hail day maximum in Europe occurs at the end of June with 531 days, and the number of hail days remains high until mid-July with approximately 400 during the 10-day moving average centered around 19 July. The higher lapse rate associated with the peak in solar radiation during long daytime

330 in the summer combined with southwesterly flows, advection of moist and warm air, and orographic effects may explain the peak (Ludlam, 1980; Punkka and Bister, 2005; Changnon and Changnon, 2000). Between the end of summer and the end of fall, the number of hail days decreases again. Unfavorable environments, such as lower near-surface temperatures and the absence of large-scale lifting are the main keys that inhibit convection.

Subdomain IDF likewise show an increased hail frequency during the summertime with up to 271 days, mainly at the

335 beginning of July. This subdomain is under the influence of the Atlantic ocean (Cantat, 2004), where trough advecting moist air to Europe are prevailing ambient conditions for severe hailstorms in West Europe (Vinet, 2001; Berthet et al., 2013. This domain also includes complex terrain such as the low Parisian Basin compared to the upper part of the arc-shaped Massif Central with higher terrain gradients that may explain the contrast between the hail-peak located in the Massif Central, which is approximately twice as high compared to the peak nearby the Morvan. Within this subdomain, the number of hail days

340 increases slightly until the peak with a local maximum in the middle of May (around 200 hail days). Spring hailstorms may be associated with subtropical air masses coming from Spain, while some summer storms preferably form ahead of cold fronts (Berthet et al., 2011). The number of hail days decreases sharply from the hail-peak season toward the end of September.

Subdomain MAQUI, located in the very southwest of France, has a very broad hail peak in the middle of June with 214 hail days during the 10-day moving average centered around 19 June. Afterwards, the number of hail days slightly decreases, thus

345 showing a right-skewed distribution. This maximum found in June differs from the analysis of Dessens et al. (2015), who found that May is the most active month of the year followed by July over the southwestern part of France and the Mediterranean area (situated along the Rhone valley). Fraile et al. (2003) and Hermida et al. (2013) found that May is the month with the highest hail kinetic energy in southwest France. Reasons for this discrepancy can be due to a longer period analyzed by Dessens et al. (2015), Hermida et al. (2013) and Fraile et al. (2003), who focused on a time range starting from the 90s, rather than in this

350 study, and by the use of hail pads in southwest France. Furthermore, the scattered network of hail pads is denser near the subdomains influenced by maritime air mass.

The number of hail days in subdomain NBEL, covering the north of France as well as the upper western part of Belgium, peaks at the end of June. Northern France and Belgium have a maritime climate influenced by the North Sea, with colder summers. Furthermore, sea-breezes and associated flow convergence zones may explain the peak at the beginning of the
355 summer (Azorin-Molina et al., 2009). In Belgium, sea-breezes preferably occur in spring or summer (Damato et al., 2003), when the temperature difference between land and ocean is most significant. A 10-years radar-based climatology conducted over Belgium by Lukach and Delobbe (2013) confirmed May and June to be the most favorable months for hail.

Subdomain BAVAR, located in southeast Germany, has the maximum of hail days at the end of July, later in the year than the other subdomains. This peak occurs when convective activity due to local conditions (local winds, uplifts) and larger-scale
360 conditions (e.g., temperature advection) are the highest (increase of wind shear, low-level convergence). Kunz and Puskeiler (2010) and Puskeiler (2013) also found that July is the month with the highest number of hail days in central and southern Germany. Interestingly, the number of hail days remains almost constant between the beginning of June and mid-August.

The diurnal cycle of hailstorms shown in Figure 8 is determined from the times where the CCTA2D detects the first radar reflectivity of 55 dBZ or more. Since the local time (LT) varies through Europe with approximately one hour from Brittany
365 in France to Saxony in Germany, all times originally given in UTC are converted to LT, representing four minutes per degree of longitude. All graphs in Figure 8 show a high variability, but some similarities can be identified. Hail is principally more frequent during the afternoon (13 to 18 LT) than during the night and early morning (midnight to 10 LT). The number of days with hail after 10 LT highly increase in almost all graphs, until the peak of hail in the afternoon.

Some discrepancies appear in the daily cycle mainly depending on where the subdomain is located, whether it's more near
370 the coast or including mountainous regions. Hailstorms in subdomain NBEL situated along the North Atlantic (but also in all other subdomains and Mediterranean coastlines, as well as the North and Baltic Sea coastlines, not shown) start principally at the beginning of the afternoon (13-15 LT). The earliest peak is reached very early at 13 LT in subdomain 6 over Brittany (not shown) and increase until 15 LT in the subdomains NBEL located over Belgium and BAVAR over southeast Germany.

Contrary to subdomains located along coastlines, domains MCEN over the Massif Central and IDF in north central France
375 peaks one hour later at 16 LT than subdomains NBEL and BAVAR. The peak during the late afternoon for more continentally characterized regions is presumably due to local orographic effects, such as slope or valley winds increasing with insulation around orography (Nesbitt and Zipser, 2003).

For subdomain MAQUI, located in southern France between the Atlantic Ocean and the Pyrenees Mountains, the peak appears very later at 19 LT. This may be due to the natural barrier of the Pyrenean Mountains, which block convective storms
380 from reaching the subdomain and suppress hail formation on the southern foothills of the mountains during the afternoon. On the northern foothills of subdomain MAQUI, flow convergence associated with local winds may lead to the formation of updrafts. Another plausible effect is that severe storms may develop from pre-existing scattered thunderstorms that form during the afternoon as was found by Nisi et al. (2016) and Nisi et al. (2018) to be decisive for the hailstorm maximum in the evening in the Ticino in southern Switzerland.

385   Some literature exists regarding the diurnal cycle of hail in Europe (Punge and Kunz, 2016). Bedka (2011), for example, recognize a diurnal cycle of overshooting tops (a small intrusion of air into the lower stratosphere related to the high velocity of the updraft) that varies with the presence of orography and/or to the distance to the sea. Kaltenböck et al. (2009) found a principal peak of hail through Europe in the middle of the afternoon. This is also the case in Poland (Twardosz et al., 2010), or in Macedonia (Dimitrievski, 1983) where the peak is reached between 14 and 17 LT. According to Martín et al. (2010),

390 hail maximum in Spain occurs between 15 and 18 LT. Kunz and Puskeiler (2010) identified a maximum in the number of damaging hail events during the afternoon (13-18 LT) for the southwestern part of Germany. The same cycle is found in the Alpine regions such as in Italy (Morgan, 1973) or in Switzerland (Nisi et al., 2016), where the maximum of hail occurs in the late afternoon and the minimum in the morning according to their radar data analysis.

    Lukach et al. (2017) demonstrated for southeast Belgium that hail falls mostly during 15-16 UTC, which is in accordance to

395 the daily cycle in subdomain 3 that includes Belgium. As for subdomain 12 in this study, Mallafré et al. (2009) found a peak later in the afternoon, around 18 LT.

4.4   Onset of SCS

To compare the spatial distribution of hailstorms during the night and day and to distinguish between convection being triggered within the boundary layer occurring preferably in the afternoon and early evening, we spatially analyzed the first detected signal

400 of the radar-derived hailstorm tracks. Figure 9 shows exemplarily the spatial distribution of track onsets at 02 and 18 LT. As expected already from the daily cycles presented in Figure 8, the occurrence probability during the night is much lower than during the day (227 onsets at 02 LT compared to more than 750 at 18 LT). Furthermore, during nighttime the location of the onsets spreads more or less randomly along coastlines and the continent without any recognizable structure. Local-scale flow effects such as the sea breeze during the night may affect the triggering of convective cells near the coastlines, which may be

405 reinforced over the Mediterranean as well as the Atlantic coastlines (Simpson, 1994). In contrast, onsets at 18 LT form several systematic patterns particularly near mountains, such as the Massif Central, the pre-Alpine domain in southern Germany, or near the French Pyrenees. Local effects, such as low-level flow convergence, and orographic effects, combined with large-scale features (fronts, large-scale lifting) may contribute to the reinforcement and development of convective cells near the mountain ranges.

410 ### 4.5   Main characteristics of hail swaths

In the following section, the main characteristics of all hail swaths occurring in France, Germany, Luxembourg, and Belgium are investigated. Hail streak length here is defined as the distance in kilometers between the start and the end of a track determined by CCTA2D, i.e., the period where a threshold of 55 dBZ is reached or exceeded. The histogram of the estimated lengths presented in Figure 10a show a high variability. The distribution follows an approximately exponential function with a

415 significant maximum for the first class. In general, the mean length (with standard deviation) is 41.5 ± 36.4 km and the median is 29.5 km. Hailstreaks located in Germany have a mean length of 39.1 ± 33 km and a median of 27 km. This mean length in France increase up to 43.9 ± 39.8 km and 32 km for the median. In total, 43% of all recorded storms over Western Europe

possess a length between 1 and 10 km. Trajectories having a length between 10.1 and 20 km decrease sharply to 19% of the overall sample of trajectories. After that, the occurrence of storms possessing longer lengths decreases slightly. Approximately

420 30% of all streaks occur with lengths between 20.1 and 150 km. Less than 8% have a length greater than 150 km. The longer tracks can be expected for highly-organized convective systems, such as MCS, including squall lines, or supercells. Only a few authors described and analyzed hailstreak characteristics in West Europe, and only very few studies based their investigations over a sufficiently long period. Puskeiler (2013), for example, investigated the hailstreak length on a radar basis in Germany during 2005 and 2011 and found a mean length of 48 km with a strong decrease for longer streaks, inducing a high standard

425 deviation of 46.7 km and a median of 40 km. Dessens (1986) found a mean length of 80 km for a small sample of 30 hailstorms in Southwest France. For Spain, Mallafré et al. (2009) determined a mean hailstreak length of around 50 ± 20 km.

The occurrence rate of hail track durations is in accordance with the length, and also decreases almost exponentially with a peak at 30 minutes (not shown). As for the other physical characteristics, long-lived swaths are rare: only 2.4% of all cells persist over 5 hours (Fluck, 2018). The width, expressed as the maximum diameter of the largest reflectivity core (≥ 55 dBZ)

430 during a hailstorm or the longest distance between two cores evolving laterally, in cases of cell-merging or splitting, show approximately a Gaussian distribution. The peak is between 9 and 10 km (41% of all events; not shown). However, as only the largest width of each swath is recorded, the results may be overestimated.

The mean angle shown in Figure 10b represents the mean orientation of a storm trajectory, and is the angle recorded by CCTA2D at the center of a swath, as most storm trajectories are approximately linear. The orientation is defined as the angle

435 between the line intersecting the reflectivity core centers, before and after the central point of a swath, to the azimuth. With this method, three time steps (i.e., 10 minutes) must exist for a track to be recorded. For slight arc-shaped trajectories, central orientation may not be accurately represented. However, only a few tracks are curved so that this effect can be neglected. The maximum occurrence (19.3%) is found in the propagation direction between 220 and 240°, i.e., a southwest direction. Around half (51%) of the hailstorms come from a west-southwest direction between 200 and 260°. Only 2.8% of the swaths have a

440 northwesterly direction. The principal southwesterly swath orientation found in the statistics confirmed previous results, such as that in the study of Puskeiler (2013), who found the highest number of hail days in southwest Germany with swaths oriented in southwesterly direction. In the Aquitaine region in France, Berthet et al. (2013) found that between 1952 and 1980 severe hailfalls came from a southwesterly direction with a mean angle of 241°.

5 Conclusions

445 This paper presents the first high resolution, radar-based hail statistics for France, Germany, Belgium, and Luxembourg over a 10-years period. A European radar composite was created from national radar composites with a five minute time step and corrected with lightning data in addition. Tracks of SCS were reconstructed using the tracking algorithm CCTA2D. Only grid points exceeding the Mason Mason (1971) criterion for hail (for reflectivity values above or equal to 55 dBZ) were used for the hail assessment. From the spatial analyses of the hail signals, the following main results are obtained:

450   – The frequency of hailstorms shows a very large spatial variability across the investigation area. In general, there is a coast-to-continental increase in the number of hail days. While none or only several radar-derived hail days occurred in the northern parts of Germany, Brittany or along the European coastlines (0-2 hail days), the number of hail days far off the coasts is much higher.

455   – Most of the hail hot spots are found on the leeward side of low-mountain ranges such as the Massif Central in France, or along the foothills such as the Swabian Jura in Germany. This is also the case for the SCS track density. The high spatial variability in the number of radar-derived hail days and the increasing number around orographic structures suggest a strong relationship between hailstorm occurrence and flow conditions induced or invigorated by to orography such as a flow-around regime with subsequence flow convergence on the lee side.

        – On the regional-scale, significant differences in the seasonal and diurnal cycles of hail occurrences are found across
460   Europe: In southwest France, for instance, the hail maximum is in mid-June, but two months later in August in eastern Germany.

Our radar-derived hail frequency estimations and maps have, of course, several limitations and uncertainty. First, due to the local-scale nature of hailstorms and the lack of accurate observations, statistics are difficult to assess and validate. No homogeneous observing system for hail exists over the entire investigation region, but only some local networks, for example,
465   the hail pad network over the southwest, central, and southern France operated by ANELFA. Similarly, direct observation networks do not exist in Belgium, Luxembourg, and Germany. The use of radar and lightning data only allows obtaining hail proxies. In particular, 2D radar data does not consider the vertical extent of reflectivity cores or echotop height as provided by 3D radar data. The radar coverage over Western Europe is reliable, but several regions are still not covered, such as the Alpine chain. This leads to a data gap in the final composite. Limited radar coverage also exists in the southeastern part of Germany
470   and near Lake Constance, leading to an underestimation of the hail potential in these regions.

Despite various errors in the radar data, such as the use of 2D data, and some gaps in radar coverage, the final results are in good accordance to other studies such as those in Germany based on 3D radar data (Puskeiler, 2013, Puskeiler et al., 2016, Schmidberger, 2018). The distribution of hail in Western Europe is also similar to larger-scale structures based on satellite-estimated hail probability as described by Punge et al. (2014) or Punge et al. (2017).

475   In the future, the results can be improved by considering longer periods, especially in the subdomains highly exposed to hail. More accurate detections of hail can be achieved, especially in mountainous terrains, using new X-band radar in the Alps. Detailed investigations or simulations with numerical weather prediction models of the flow conditions depending on atmospheric conditions may help to find robust evidence of the flow-around regime that may be decisive for the increased hail frequency downstream of several low mountain ranges. This can help to better understand the effects of orography on the
480   triggering of convection.

Data availability. 2D radar data for Germany can be accessed via the German Weather Service (DWD) ftp server while French national radar composites are available upon request to the French Meteorological Service (Météo-France). SCS/hail tracks were computed on radar data and are only available upon request to M. Kunz. ESWD reports are available at: www.eswd.eu. ERA-Interim data can be downloaded from the ECMWF server.

485 *Author contributions.* EF edited most part of the paper, performed the statistical analyses and computed the SCS/hail tracks. MK verified in details the analytical methods and results, added crucial suggestions to the paper and contributed to the editing/revision of the manuscript. PG and SR added contructive suggestions to the paper. MK supervised the project in collaboration with PG and SR.

Competing interests. The authors declare that they have no conflict of interest.

Acknowledgements. The authors thank the French Meteorological Service (Météo-France) and the German Weather Service (DWD) for
490 providing long-term radar data, Siemens AG (S. Thern) for providing lightning data, and the ESWD for archiving hail reports. The authors also acknowledge Tokio Millennium Re Ltd for funding the project.
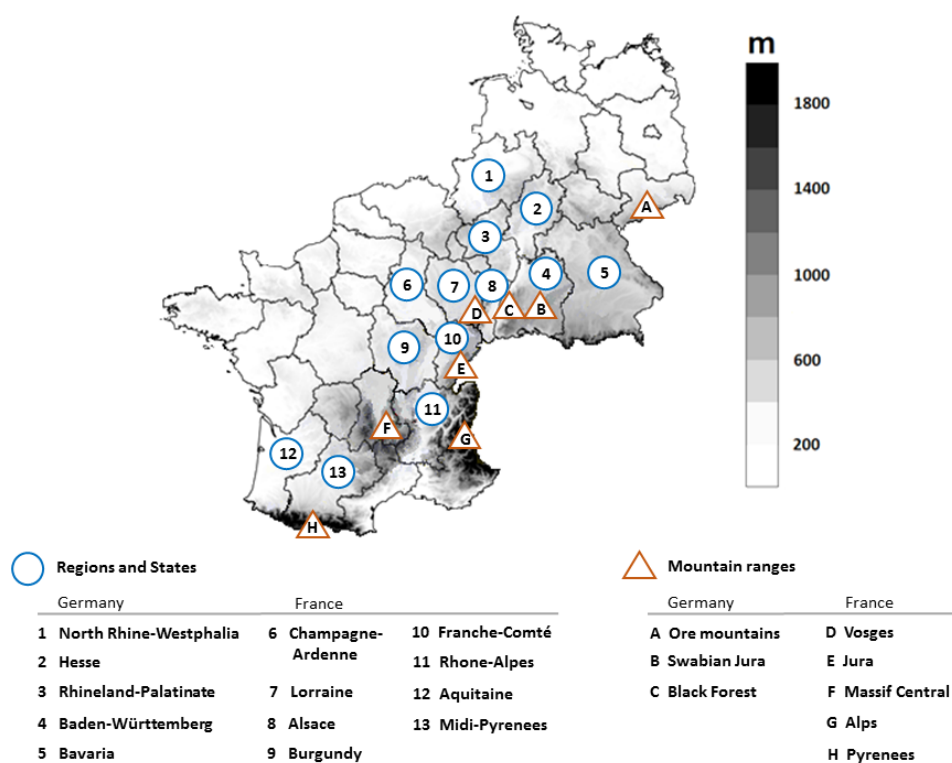
Figure 1. European regions and mountain ranges mentioned in this study.
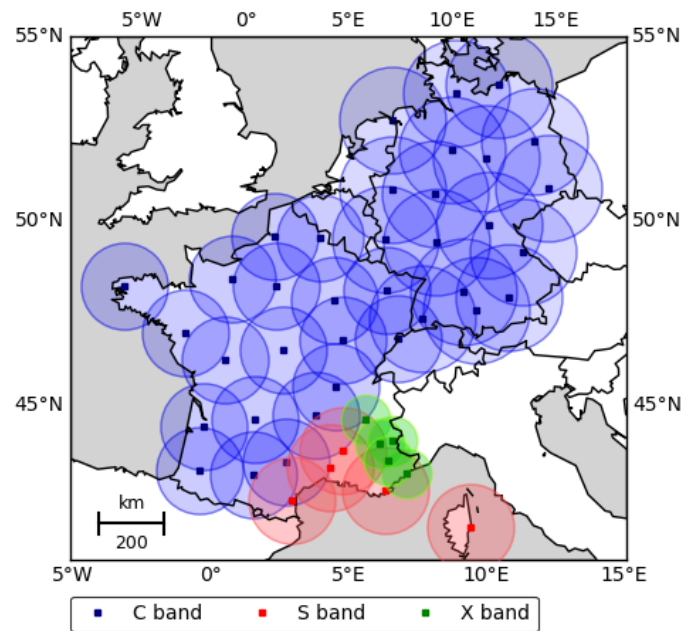
Figure 2. Locations (squares) and coverage of the radar stations (circles) in 2015 used in this study. See text for further explanations.
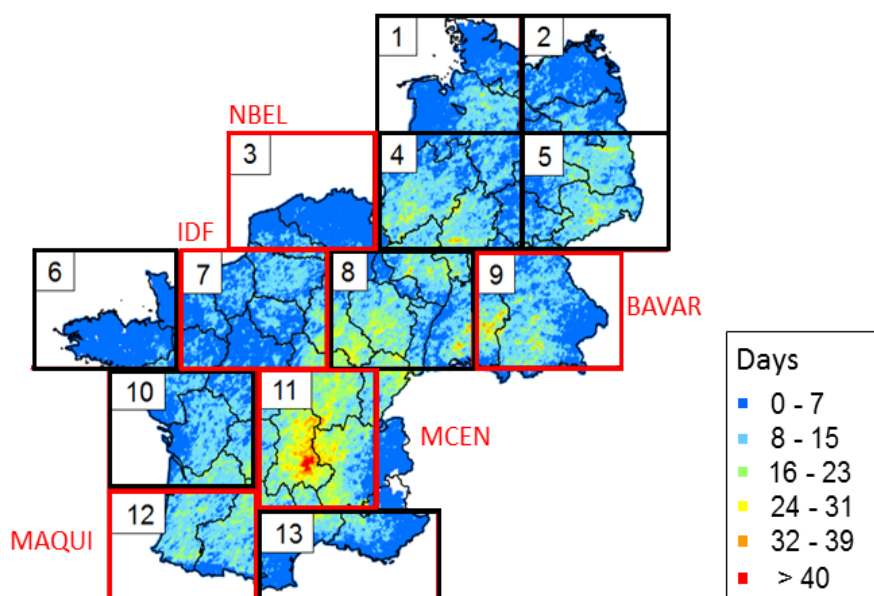
Figure 3. Number of radar-derived hail days for 1×1 km^2 grid points in France, Germany, Belgium, and Luxembourg between 2005 and 2014. Squares represent boundaries of subdomains further investigated in this study (See subsection 4.3 for further details). Special emphasis is given for subdomains delimited in red.
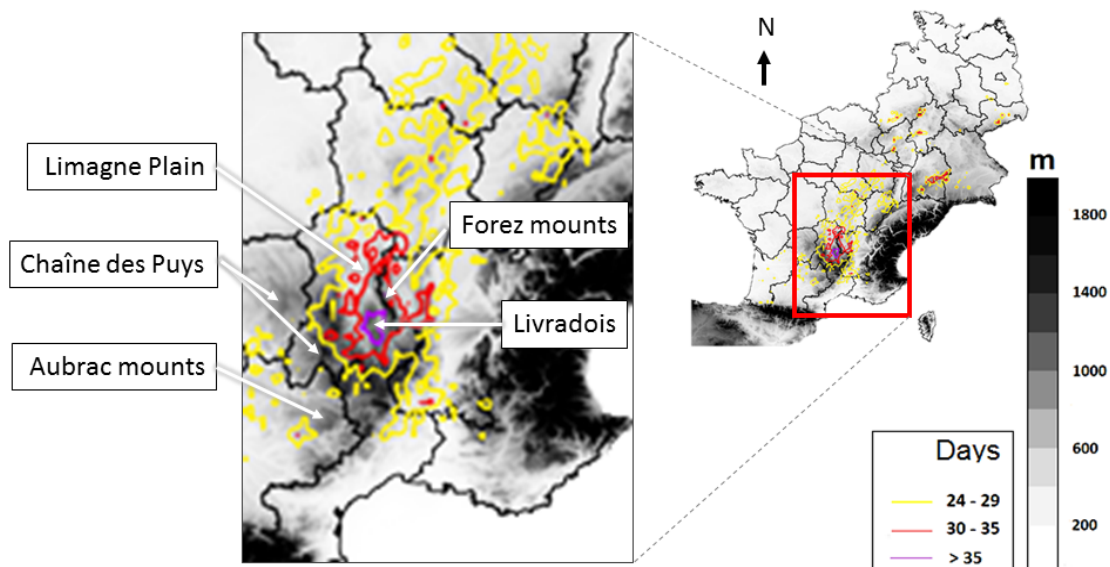
Figure 4. Contours of radar-derived hail days from 2005 to 2014 overlaid with the orography.
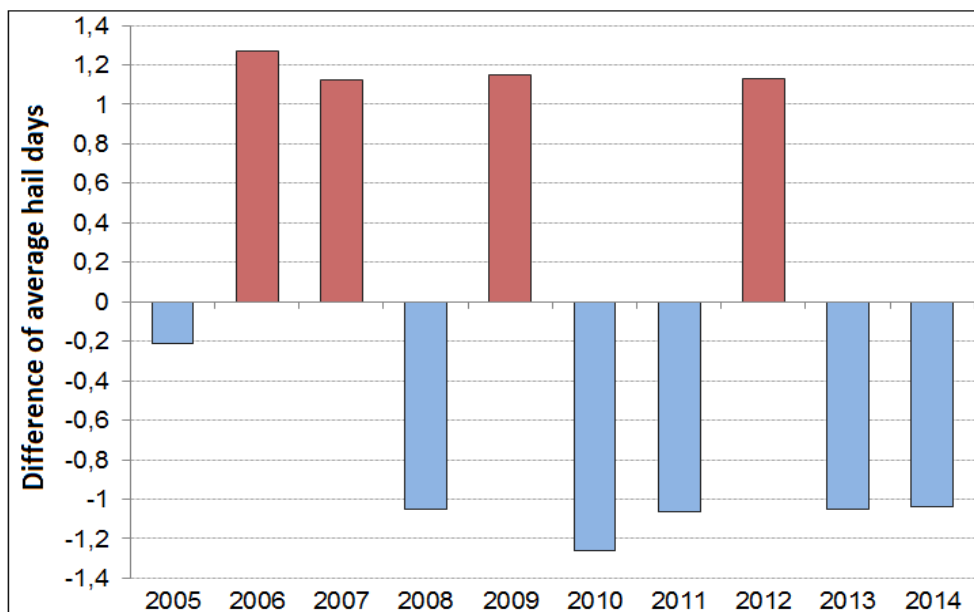
Figure 5. Anomalies of annual mean hail days with respect to the overall mean of hail days from 2005 to 2014.
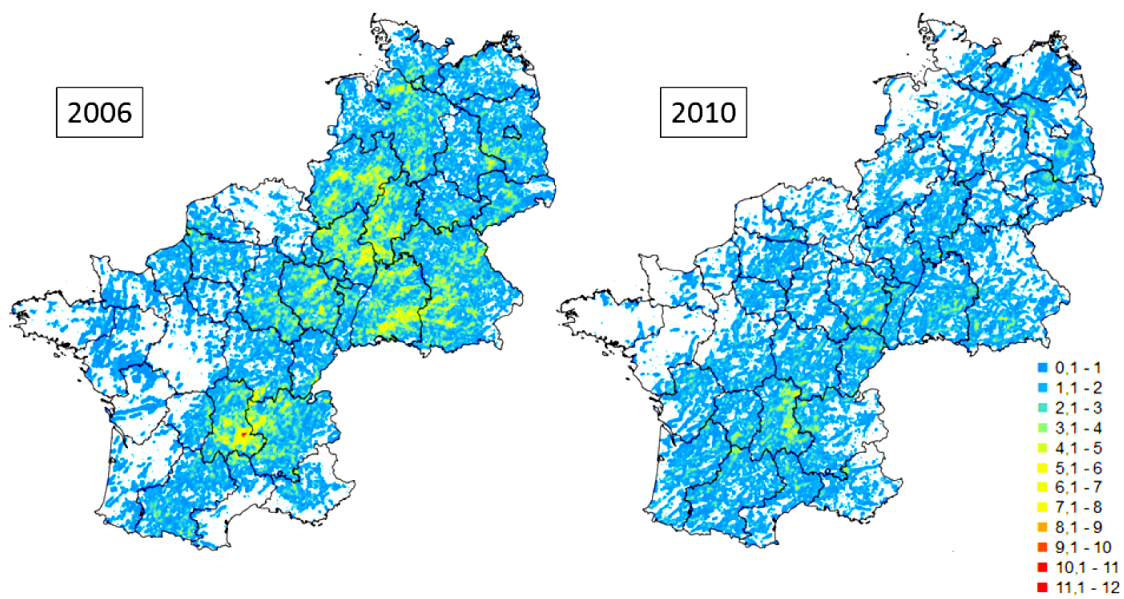
Figure 6. Number of radar-derived hail days exemplary shown for the years with the highest (2006, left) and lowest (2010, right) hail day frequency.
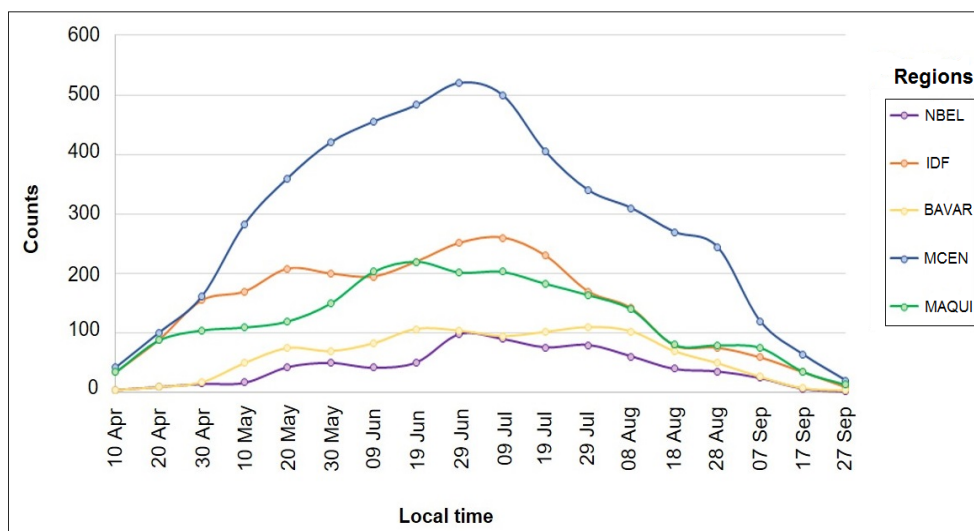
Figure 7. Time-series of radar-derived hail days (10-days moving average denoted as counts) for the subdomains NBEL, IDF, BAVAR, MCEN and MAQUI shown in Figure 8.
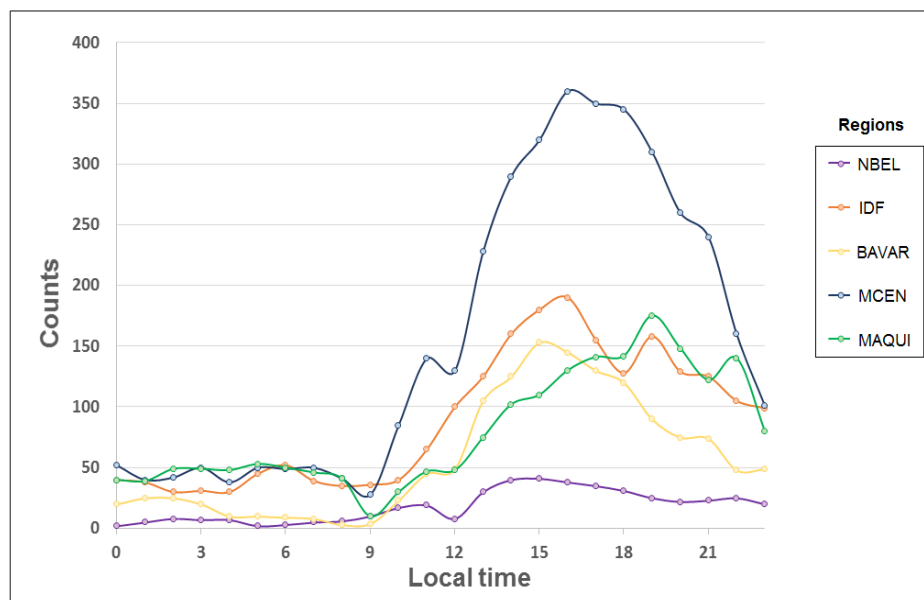
Figure 8. Hourly distribution of radar-derived hail days for each subdomain
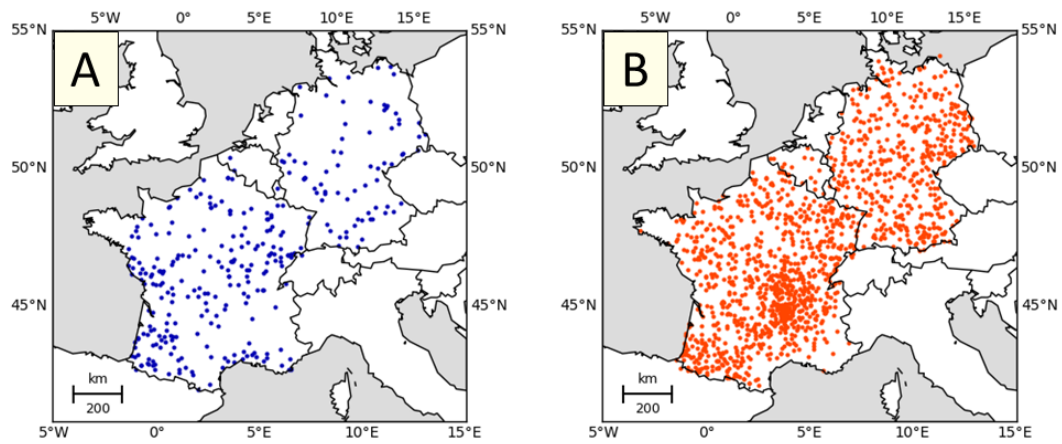
Figure 9. Locations of the first convective signatures detected by CCTA2D at 02 LT (A) and 18 LT (B).
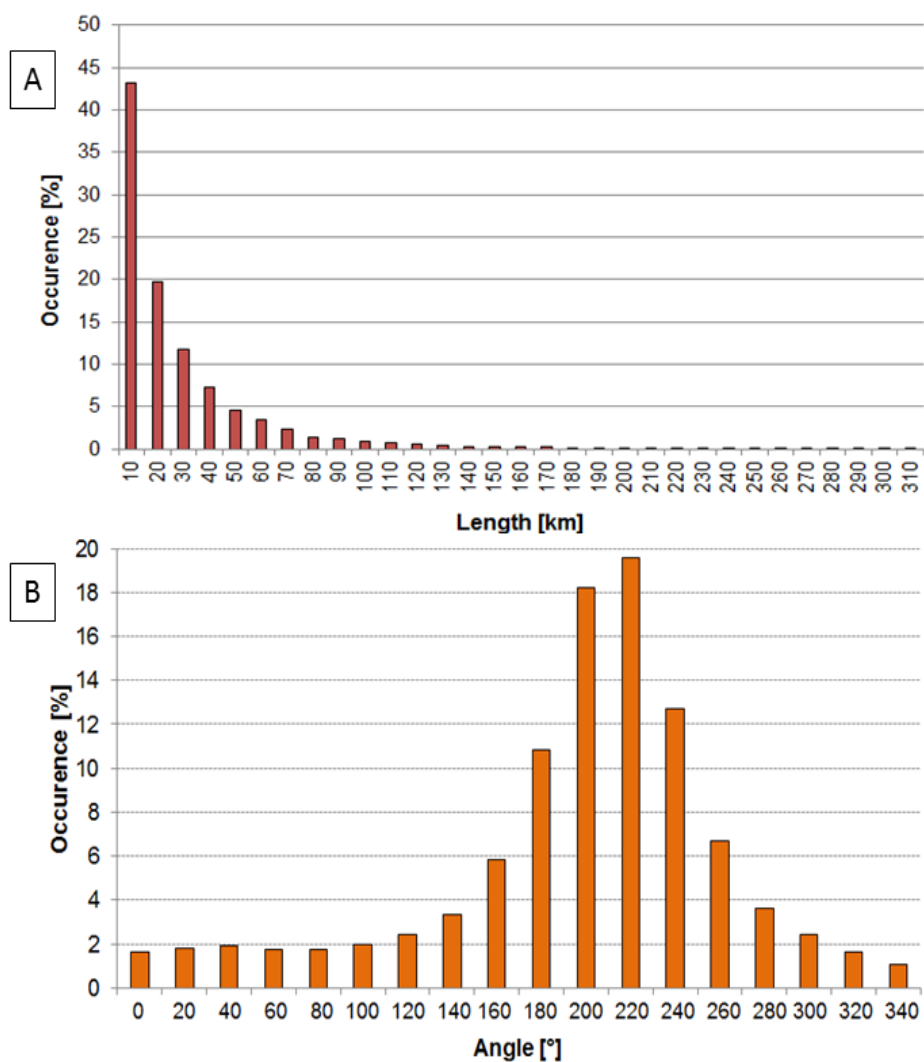
Figure 10. Histograms of all SCS mean length (A) and mean orientation (B).

References

Azorin-Molina, C., Connell, B. H., and Baena-Calatrava, R.: Sea-breeze convergence zones from AVHRR over the Iberian Mediterranean area and the Isle of Mallorca, Spain, J. Appl. Meteorol., 48, 2069–2085, https://doi.org/https://doi.org/10.1175/2009JAMC2141.1, 2009.

Bastin, S., Drobinski, P., Dabas, A., Delville, P., Reitebuch, O., and Werner, C.: Impact of the Rhône and Durance valleys on sea-breeze circulation in the Marseille area, Atmos. Res., 74, 303–328, https://doi.org/https://doi.org/10.1016/j.atmosres.2004.04.014, 2005.

Baughman, R. and Fuquay, D.: Hail and lightning occurrence in mountain thunderstorms, J. Appl. Meteorol., 9, 657–660, https://doi.org/https://doi.org/10.1175/1520-0450(1970)009<0657:HALOIM>2.0.CO;2, 1970.

Bedka, K.: Overshooting cloud top detections using MSG SEVIRI Infrared brightness temperatures and their relationship to severe weather over Europe, Atmos. Res., 99, 175–189, https://doi.org/https://doi.org/10.1016/j.atmosres.2010.10.001, 2011.

Berthet, C., Dessens, J., and Sanchez, J. L.: Regional and yearly variations of hail frequency and intensity in France, Atmos. Res., 100, 391–400, https://doi.org/https://doi.org/10.1016/j.atmosres.2010.10.008, 2011.

Berthet, C., Wesolek, E., Dessens, J., and Sanchez, J. L.: Extreme hail day climatology in Southwestern France, Atmos. Res., 123, 139–150, https://doi.org/https://doi.org/10.1016/j.atmosres.2012.10.007, 2013.

Cantat, O.: Analyse critique sur les tendances pluviométriques au 20eme siècle en Basse-Normandie: Réfléxions sur la fiabilité des données et le changement climatique, Climatol., 1, 11–32, https://doi.org/https://doi.org/10.4267/climatologie.963, 2004.

Caylor, I. and Chandrasekar, V.: Time-varying ice crystal orientation in thunderstorms observed with multiparameter radar, Trans. Geosci. Remote Sens., 34, 847–858, https://doi.org/https://doi.org/10.1109/36.508402, 1996.

Changnon, S. and Changnon, D.: Long-term fluctuations in hail incidences in the United States, J. Climate, 13, 658–664, http://journals.ametsoc.org/doi/abs/10.1175/1520-0442%282000%29013%3C0658%3ALTFIHI%3E2.0.CO%3B2, 2000.

Changnon, S. A.: The scales of hail, J. Appl. Meteorol., 16, 626–648, https://doi.org/https://doi.org/10.1175/1520-0450(1977)016<0626:TSOH>2.0.CO;2, 1977.

Changnon, S. A.: Data and approaches for determining hail risk in the contiguous United States, J. Appl. Meteorol., 38, 1730–1739, https://doi.org/https://doi.org/10.1175/1520-0450(1999)038<1730:DAAFDH>2.0.CO;2, 1999.

Chappell, C. F.: Quasi-stationary convective events, Springer, London, https://link.springer.com/chapter/10.1007/978-1-935704-20-1_13, 1986.

Damato, F., Planchon, O., and Dubreuil, V.: A remote-sensing study of the inland penetration of sea-breeze fronts from the English Channel, Weather, 58, 219–226, https://doi.org/https://doi.org/10.1256/wea.50.02, 2003.

Deepen, J.: Schadenmodellierung extremer Hagelereignisse in Deutschland, Master's thesis, Institut für Landschaftsökologie der Westfälischen Wilhelms-Universität Münster, https://doi.org/https://www.uni-muenster.de/imperia/md/content/landschaftsoekologie/klima/pdf/2006_deepen_dipl.pdf, 2006.

Dessens, J.: Hail in Southwestern France. I: Hailfall Characteristics and Hailstrom Environment, J. Clim. Appl. Meteorol., 25, 35–47, https://doi.org/https://doi.org/10.1175/1520-0450(1986)025<0035:HISFIH>2.0.CO;2, 1986.

Dessens, J., Berthet, C., and Sanchez, J.: Change in hailstone size distributions with an increase in the melting level height, Atmos. Res., 158, 245–253, https://doi.org/https://doi.org/10.1016/j.atmosres.2014.07.004, 2015.

DeutscheRück: Sturmdokumentation 2012 Deutschland, Tech. rep., Deutsche Rückversicherung, https://www.deutscherueck.de/fileadmin/user_upload/WEB_Sturmdoku_2012.pdf, 2013.

Dimitrievski, V.: Characteristics of hail processes and hail falls in Macedonia, J. Weather Modif., 1, 62–63, http://www.journalofweathermodification.org/index.php/JWM/article/view/90/74, 1983.

530   Dotzek, N., Groenemeijer, P., Feuerstein, B., and Holzer, A. M.: Overview of ESSL's severe convective storms research using the European Severe Weather Database ESWD, Atmos. Res., 93, 575–586, https://doi.org/https://doi.org/10.1016/j.atmosres.2008.10.020, 2009.

Fluck, E.: Hail statistics for European countries, Ph.D. thesis, Karlsruhe Institute of Technology, https://pdfs.semanticscholar.org/74b5/2e00fd4d299e40011d73aa596c6846212252.pdf, 2018.

Fouillet, A., Rey, G., Wagner, V., Laaidi, K., Empereur-Bissonnet, P., Le Tertre, A., Frayssinet, P., Bessemoulin, P., Laurent, F., De Crouy-

535   Chanel, P., et al.: Has the impact of heat waves on mortality changed in France since the European heat wave of summer 2003? A study of the 2006 heat wave, Int. J. Epidem., 37, 309–317, https://doi.org/https://doi.org/10.1093/ije/dym253, 2008.

Fraile, R., Castro, A., and Sánchez, J. L.: Analysis of hailstone size distributions from a hailpad network, Atmos. Res., 28, 311–326, https://doi.org/https://doi.org/10.1016/0169-8095(92)90015-3, 1992.

Fraile, R., Berthet, C., Dessens, J., and Sánchez, J. L.: Return periods of severe hailfalls computed from hailpad data, Atmos. Res., 67,

540   189–202, https://doi.org/https://doi.org/10.1016/S0169-8095(03)00051-6, 2003.

Gourley, J. J., Tabary, P., and Parent du Chatelet, J.: Data quality of the Meteo-France C-band polarimetric radar, J. Atmos. Ocean. Technol., 23, 1340–1356, https://doi.org/https://doi.org/10.1175/JTECH1912.1, 2006.

Gudd, M.: Gewitter und Gewitterschäden im südlichen hessischen Berg-und Beckenland und im Rhein-Main-Tiefland 1881 bis 1980: eine Auswertung mit Hilfe von Schadensdaten, Ph.D. thesis, University of Mainz, https://publications.ub.uni-mainz.de/theses/volltexte/2004/

545   523/pdf/523.pdf, 2003.

Handwerker, J.: Cell Tracking with TRACE3D: a New Algorithm, Atmos. Res., 61, 15–34, https://doi.org/https://doi.org/10.1016/S0169-8095(01)00100-4, 2002.

Hermida, L., Sánchez, J. L., López, L., Berthet, C., Dessens, J., García-Ortega, E., and Merino, A.: Climatic trends in hail precipitation in France: spatial, altitudinal, and temporal variability, Sci. World. J., 2013, https://doi.org/https://doi.org/10.1155/2013/494971, 2013.

550   Hermida, L., López, L., Merino, A., Berthet, C., García-Ortega, E., Sánchez, J. L., and Dessens, J.: Hailfall in Southwest France: Relationship with precipitation, trends and wavelet analysis, Atmos. Res., 156, 174–188, https://doi.org/https://doi.org/10.1016/j.atmosres.2015.01.005, 2015.

Hohl, R.: Relationship between hailfall intensity and hail damage on ground, determined by radar and lightning observations, Ph.D. thesis, Departement of Geography, University of Fribourg, Switzerland, https://doc.rero.ch/record/5136/files/1_HohlRM.pdf, 2001.

555   Hohl, R., Schiesser, H.-H., and Aller, D.: Hailfall: the relationship between radar-derived hail kinetic energy and hail damage to buildings, Atmos. Res., 63, 177–207, https://doi.org/https://doi.org/10.1016/S0169-8095(02)00059-5, 2002.

Junghänel, T., Brendel, C., Winterrath, T., and Walter, A.: Towards a radar- and observation-based hail climatology for Germany, Meteorol. Z., 25, 435–445, https://doi.org/10.1127/metz/2016/0734, 2016.

Kaltenböck, R., Diendorfer, G., and Dotzek, N.: Evaluation of thunderstorm indices from ECMWF analyses, lightning data and severe storm

560   reports, Atmos. Res., 93, 381–396, https://doi.org/https://doi.org/10.1016/j.atmosres.2008.11.005, 2009.

Koebele, D.: Analyse von Konvergenzbereichen bei Hagelereignissen stromab von Mittelgebirgen anhand von COSMO-Modellsimulationen, Master's thesis, Karlsruhe Institute of Technology, https://www.imk-tro.kit.edu/download/Masterarbeit_Koebele.pdf, 2014.

Kunz, M. and Kugel, P. I.: Detection of hail signatures from single-polarization C-band radar reflectivity, Atmos. Res., 153, 565–577, https://doi.org/https://doi.org/10.1016/j.atmosres.2014.09.010, 2015.

565   Kunz, M. and Puskeiler, M.: High-resolution Assessment of the Hail Hazard over Complex Terrain from Radar and Insurance Data, Meteorol.
        Z., 19, 427–439, https://doi.org/https://doi.org/10.1127/0941-2948/2010/0452, 2010.

       Kunz, M., Blahak, U., Handwerker, J., Schmidberger, M., Punge, H. J., Mohr, S., Fluck, E., and Bedka, K. M.: The severe hailstorm
        in SW Germany on 28 July 2013: Characteristics, impacts, and meteorological conditions, Q. J. R. Meteorol. Soc., 144, 231–250,
        https://doi.org/https://doi.org/10.1002/qj.3197, 2018.

570   Ligda, M. G.: The radar observation of lightning, J. Atmos. Terr. Phys., 9, 309–346, https://doi.org/https://doi.org/10.1016/0021-
        9169(56)90152-0, 1956.

       Ludlam, F. H.: Clouds and storms: The behavior and effect of water in the atmosphere, Pennsylvania State University Press, http://agris.fao.
        org/agris-search/search.do?recordID=US8025686, 1980.

       Lukach, M. and Delobbe, L.: Radar-based hail statistics over Belgium, in: 7th European Conference on Severe Storms (ECSS), 7-13 June
575   2013, Helsinki, Finland, 2013.

       Lukach, M., Foresti, L., Giot, O., and Delobbe, L.: Estimating the occurrence and severity of hail based on 10 years of observations from
        weather radar in Belgium, Meteorol. Appl., 24, 250–259, https://doi.org/https://doi.org/10.1002/met.1623, 2017.

       Mallafré, M. C., Ribas, T. R., del Carmen Llasat Botija, M., and Sánchez, J. L.: Improving hail identification in the
        Ebro Valley region using radar observations: Probability equations and warning thresholds, Atmos. Res., 93, 474–482,
580   https://doi.org/https://doi.org/10.1016/j.atmosres.2008.09.039, 2009.

       Martín, J. A. G., Hijano, C. F., Jara, J. C. M., Cardineau, C. A., Fernández, A. F., and Piserra, M. T.: Tormentas con pedrisco en Castilla-La
        Mancha: estudio sobre los eventos de granizo en el periodo 1850-1950 y desarrollo de una base de datos y su implantación en un SIG
        aplicado a la región, Segur. Medio. Ambi., pp. 32–45, https://www.fundacionmapfre.org/documentacion/publico/i18n/catalogo_imagenes/
        grupo.cmd?path=1062523, 2010.

585   Mason, B.: The physics of clouds, Oxford University Press, Oxford, https://doi.org/https://doi.org/10.1002/qj.49709841723, 1971.

       Merino, A., García-Ortega, E., López, L., Sánchez, J., and Guerrero-Higueras, A.: Synoptic environment, mesoscale
        configurations and forecast parameters for hailstorms in Southwestern Europe, Atmos. Res., 122, 183–198,
        https://doi.org/https://doi.org/10.1016/j.atmosres.2012.10.021, 2013.

       Mohr, S. and Kunz, M.: Recent trends and variabilities of convective parameters relevant for hail events in Germany and Europe, Atmos.
590   Res., 123, 211–228, https://doi.org/https://doi.org/10.1016/j.atmosres.2012.05.016, 2013.

       Mohr, S., Kunz, M., and Geyer, B.: Hail potential in Europe based on a regional climate model hindcast, Geophys. Res. Lett., 42, 10 904–
        10 912, https://doi.org/doi:10.1002/2015GL067118., 2015a.

       Mohr, S., Kunz, M., and Keuler, K.: Development and application of a logistic model to estimate the past and future hail potential in Germany,
        J. Geophys. Res., 120, 3939–3956, https://doi.org/10.1002/2014JD022959, 2015b.

595   Morgan, G. M.: A general description of the hail problem in the Po Valley of northern Italy, J. Appl. Meteorol., 12, 338–353, https://doi.org/
        10.1175/1520-0450(1973)012<0338:AGDOTH>2.0.CO;2, 1973.

       Nesbitt, S. W. and Zipser, E. J.: The diurnal cycle of rainfall and convective intensity according to three years of TRMM measurements, J.
        Clim, 16, 1456–1475, https://doi.org/10.1175/1520-0442(2003)016<1456:TDCORA>2.0.CO;2, 2003.

       Nisi, L., Ambrosetti, P., and Clementi, L.: Nowcasting severe convection in the Alpine region: The COALITION approach, Q. J. R. Meteorol.
600   Soc., 140, 1684–1699, https://doi.org/https://doi.org/10.1002/qj.2249, 2014.

       Nisi, L., Martius, O., Hering, A., Kunz, M., and Germann, U.: Spatial and temporal distribution of hailstorms in the Alpine region: a long-
        term, high resolution, radar-based analysis, Q. J. R. Meteorol. Soc., 142, 1590–1604, https://doi.org/https://doi.org/10.1002/qj.2771, 2016.

Nisi, L., Hering, A., Germann, U., and Martius, O.: A 15-year hail streak climatology for the Alpine region, Q. J. R. Meteorol. Soc., 144, 1429–1449, https://doi.org/https://doi.org/10.1002/qj.3286, 2018.

605 NOAA: Global Climate Report for Annual 2010, Tech. rep., National Centers for Environmental Information, https://www.ncdc.noaa.gov/sotc/global/201013, 2011.

NOAA: Global Climate Report for Annual 2013, Tech. rep., NOAA National Centers for Environmental Information, https://www.ncdc.noaa.gov/sotc/global/201313, 2014.

Piper, D. and Kunz, M.: Spatiotemporal variability of lightning activity in Europe and the relation to the North Atlantic Oscillation teleconnection pattern., Nat. Hazards Earth Syst. Sci., 17, https://doi.org/https://doi.org/10.5194/nhess-17-1319-2017, 2017.

Piper, D. A.: Untersuchung der Gewitteraktivität und der relevanten großräumigen Steuerungsmechanismen über Mittel- und Westeuropa, Ph.D. thesis, Karlsruhe Institute of Technology, https://doi.org/doi:10.5445/KSP/1000072089, 2017.

Piper, D. A., Kunz, M., Allen, J. T., and Mohr, S.: Investigation of the temporal variability of thunderstorms in Central and Western Europe and the relation to large-scale flow and teleconnection patterns, Q. J. R. Meteorol. Soc., 145, 3644–3666, https://doi.org/https://doi.org/10.1002/qj.3647, 2019.

Pohjola, H. and Mäkelä, A.: The comparison of GLD360 and EUCLID lightning location systems in Europe, Atmos. Res., 123, 117–128, https://doi.org/https://doi.org/10.1016/j.atmosres.2012.10.019, 2013.

Punge, H. and Kunz, M.: Hail observations and hailstorm characteristics in Europe: A review, Atmos. Res., 176, 159–184, https://doi.org/https://doi.org/10.1016/j.atmosres.2016.02.012, 2016.

620 Punge, H., Bedka, K., Kunz, M., and Werner, A.: A new physically based stochastic event catalog for hail in Europe, Nat. Hazards, 73, 1625–1645, https://doi.org/https://doi.org/10.1007/s11069-014-1161-0, 2014.

Punge, H., Bedka, K., Kunz, M., and Reinbold, A.: Hail frequency estimation across Europe based on a combination of overshooting top detections and the ERA-INTERIM reanalysis, Atmos. Res., 198, 34–43, https://doi.org/doi:10.1016/j.atmosres.2017.07.025, 2017.

Punkka, A.-J. and Bister, M.: Occurrence of summertime convective precipitation and mesoscale convective systems in Finland during 2000–01, Mon. Wea. Rev., 133, 362–373, https://doi.org/https://doi.org/10.1175/MWR-2854.1, 2005.

Puskeiler, M.: Radarbasierte Analyse der Hagelgefährdung in Deutschland, Ph.D. thesis, Karlsruhe Institute of Technology, http://www.imk-tro.kit.edu/download/Dissertation_Puskeiler_Marc.pdf, 2013.

Puskeiler, M., Kunz, M., and Schmidberger, M.: Hail statistics for Germany derived from single-polarization radar data, Atmos. Res., 178, 459–470, https://doi.org/https://doi.org/10.1016/j.atmosres.2016.04.014, 2016.

630 Rädler, A. T., Groenemeijer, P., Faust, E., and Sausen, R.: Detecting Severe Weather Trends Using an Additive Regressive Convective Hazard Model (AR-CHaMo), J. Appl. Meteorol., 57, 569–587, https://doi.org/https://doi.org/10.1175/JAMC-D-17-0132.1, 2018.

Schmidberger, M.: Hagelgefährdung und Hagelrisiko in Deutschland basierend auf einer Kombination von Radardaten und Versicherungsdaten, phdthesis, Karlsruhe Institute of Technology, https://doi.org/doi:10.5445/KSP/1000086012, 2018.

Schulz, W., Diendorfer, G., Pedeboy, S., and Poelman, D. R.: The European lightning location system EUCLID–Part 1: Performance analysis and validation, Nat. Hazards Earth Syst. Sci, 16, 595–605, 2016.

Schuster, S. S., Blong, R. J., and Speer, M. S.: A hail climatology of the greater Sydney area and New South Wales, Australia, Int. J. Climatol., 25, https://doi.org/https://doi.org/10.1002/joc.1199, 2005.

Simpson, J. E.: Sea breeze and local winds, Cambridge University Press, Cambridge, https://books.google.co.il/books?hl=en&lr=&id=6WPodgtunqIC&oi=fnd&pg=PP17&dq=Simpson,+J.+E.,+1994:Sea+breeze+and+local+winds.+Cambridge+University+Press, 640 +Cambridge,+239+pp&ots=Erev75mbTE&sig=I_BqDmgDoAFfa3stgrHYZHW_Li0&redir_esc=y#v=onepage&q&f=false, 1994.

SwissRe: Sigma: Natural- and Man-made Catastrophes 2013, Tech. rep., Swiss Re Economic Research and Consulting, https://reliefweb.int/sites/reliefweb.int/files/resources/SwisRe_2014_Natural_Catastrophes_sigma1_2014_en.pdf, 2014.

Tabary, P.: The new French operational radar rainfall product. Part I: Methodology, Wea. Forecasting, 22, 393–408, https://doi.org/https://doi.org/10.1175/WAF1004.1, 2007.

645   Twardosz, R., Niedzwiedz, T., and Lupikasza, E.: Hail thunderstorms in Cracow and their circulation determinants (1863–2008), W. Geograph. Res. University of Kielce, Kielce, pp. 295–305, http://komhydptg.geo.uni.lodz.pl/uploads/images/publikacje/kielce%202010.pdf, 2010.

Vinet, F.: Climatology of hail in France, Atmos. Res., 56, 309–323, https://doi.org/https://doi.org/10.1016/S0169-8095(00)00082-X, 2001.

Vinet, F.: La question du risque climatique en agriculture: le cas de la grêle en France/Climatic risk in agriculture: the case of hail falls in
650   France, in: Ann. Géograph., pp. 592–613, JSTOR, www.jstor.org/stable/23455979, 2002.

Waldvogel, A., Federer, B., and Grimm, P.: Criteria for the detection of hail cells, J. Appl. Meteorol., 18, 12, https://doi.org/https://doi.org/10.1175/1520-0450(1979)018<1521:CFTDOH>2.0.CO;2, 1979.

Wapler, K.: The life-cycle of hailstorms: Lightning, radar reflectivity and rotation characteristics, Atmos. Res., 193, 60–72, https://doi.org/http://doi.org/10.1016/j.atmosres.2017.04.009, 2017.

655   Weissmann, M., Braun, F. J., Gantner, L., Mayr, G. J., Rahm, S., and Reitebuch, O.: The Alpine mountain–plain circulation: Airborne Doppler lidar measurements and numerical simulations, Mon. Weather. Rev., 133, 3095–3109, https://doi.org/https://doi.org/10.1175/MWR3012.1, 2005.

Yu, N., Gaussiat, N., and Tabary, P.: Polarimetric X-band weather radars for quantitative precipitation estimation in mountainous regions, Q. J. R. Meteorol. Soc., 144, 2603–2619, https://doi.org/https://doi.org/10.1002/qj.3366, 2018.